Defocal Lens Assembly for Multi-Element Full-Duplex Free Space Optical Transceiver

A F M Saniul Haq[1]
[1]*The College of Optics and Photonics*
CREOL, University of Central Florida
Orlando, FL USA 32816
saniul.haq@knights.ucf.edu

Murat Yuksel[1,2]
[2]*Dept. of Electrical and Computer Engineering*
University of Central Florida
Orlando, FL USA 32816
murat.yuksel@ucf.edu

***Abstract*—Free-space optical communication presents a significant opportunity for next generation wireless communication and networking with high modulation speed, broad bandwidth, secure and direct line-of-sight link, and unlicensed spectrum. Multi-element free-space optical transceivers can be used to improve the overall optical link performance as they offer spatial reuse, beam steering, and tolerance to mobility. In this paper, we explore the design and analysis of a fixed effective focal length lens system and the optical coupling efficiency that can be maximized by defocusing the beam footprint on the receiver side for a full-duplex free-space optical communication link. We propose a lens system with effective focal length of 49.5 mm, F/2, and field-of-view of 28° to collimate the transmit beam onto the receiver plane. We further present how to maximize the optical coupling efficiency and vibration tolerance by introducing small defocusing length between transmitter and lens assembly.**

***Index Terms*—FSO Link, Defocused Lens System, Optical Coupling, Tolerance, Full-Duplex, Optical Transceiver**

I. Introduction

With increasing demand for high-speed data communication and wireless connectivity, free-space optical communication (FSOC) has attracted a great deal of attention for wireless communication and networking. The optical spectrum can be a suitable addition, and in some cases replacement, to the already-exhausted radio spectrum for next generation wireless communication systems. Narrow beam infrared communication, mostly implemented with lasers, opens up opportunities to connect ever-growing wireless devices, sensing applications, and large-scale Internet-of-Things (IoT) [1]. Another major application field of narrow beam infrared FSOC is the satellite communications and mobile airborne base stations. Initiatives like Project Loon [2] and Starlink satellites [3] implement laser-based FSOC to meet the ultra-high speed data demand and secure communication link. FSOC proves to be a critical technology as it provides significantly faster data exchange rate, higher spatial security, mass production capability, and lower power budget. However, direct line-of-sight (LOS) requirement and the loss induced by turbulent free-space medium limit the applicability of FSOC to indoor and short-range outdoor settings. FSOC also provides the capability of implementing ad-hoc network for future communication protocols due to its high modulation speed, broad bandwidth, unlicensed spectrum at no cost, and spatial reuse ability [4].

Mobile free-space optical (FSO) networks can be a useful solution for a wide range of scenarios, including delivering connectivity to rural and disaster-struck areas, inter-satellite communication, ad-hoc networking in crowded events, and assisting military activities in rough terrains. All of these applications require high bandwidth and secure interception-free connectivity which can be achieved by deploying mobile FSO systems. Initial prototypes of these mobile FSO systems utilized low cost, low power, and densely packaged solid state light emitting diodes (LEDs). However, due to the higher divergence angles of the transmitters, the effective optical link ranges are limited to sub-ten meters, which can be significantly improved by replacing LEDs with vertical cavity surface emitting lasers (VCSELs) as transmitters. Furthermore, the capacity of the network can be increased by implementing an in-band full-duplex (IBFD) configuration. IBFD communication uses the same wavelength to transmit and receive simultaneously. Even though IBFD communication suffers from self-interference (SI) losses, SI mitigating steps and careful design implementation can lead to increased channel capacity. Even in the presence of SI, full-duplex communication can provide at least 20% gain over half-duplex communication [5].

The disadvantages of IBFD FSOC can be addressed by implementing multi-element transceiver layout designs with capability of spatial reuse, beam steering, cognitive techniques for adaptive optimizations, and tolerance to mobility, vibration, sway, or tilt during communication. Several mechanical beam steering approaches, such as MEMS-based mirror [6], servo-based gimbal [1], liquid crystal modulators [7], optical phased arrays [8], and optical beam steering approach, such as infrared (IR) beam steering using a lens system [9], can be adopted to establish LOS for mobile FSO networks. In addition to the multi-element transceiver and mechanical beam steering techniques, a near-afocal lens assembly for the transmitter can provide tolerance to vibration and sway to ensure LOS [10].

In this paper, we address the issues of establishing an LOS optical link between mobile platforms such as UAVs, autonomous vehicles, floating/flying base stations, and stationary building-top transceivers. We propose a near-afocal lens assembly design for multi-element FSO transceiver to optimize

This work was supported in part by National Science Foundation award 2115215 and U.S. Navy SBIR program.

the received power based on link distance and transceiver layout design. The main contributions are as follows:

- An optimized design of multi-element FSO transceiver layout that includes selecting the number of transmitters and receivers, and their placement on the transceiver plane.
- An overview of the circuit design considerations taken into account to implement the FSO transceiver.
- A defocal lens assembly design for the transmitters to control the beam width and footprint at the receiver end to optimize the received power and tolerance to vibration, sway, and tilt of the mobile platform.

II. Background and Literature Review

A. Multi-Element Full-Duplex FSO Transceiver

Prior work on full-duplex FSOC has reported *out-of-band* transceiver designs. Wang *et al.* demonstrated a full-duplex indoor FSOC for error-free ($BER < 10^{-9}$) short-range operation [11]. To suppress the SI for full-duplex operation, the transceiver used different optical wavelengths for uplink (1550.12 nm) and downlink (850 nm) channels, which makes it an out-of-band design. IBFD FSOC designs have recently received attention due to their advantage over out-of-band designs. An IBFD design for full-duplex FSOC has been reported by Oh *et al.* [12], which implements communication between a stationary controller and a mobile node using beam reversibility and data erasure method. However, the controller has only a transmitter but no receiver. Johnson *et al.* proposed passive isolation of the transmitter and the receiver of a node, but no functional prototype was demonstrated [13]. In our earlier work [5], [14], we demonstrated isolation of infrared transmitter and receiver in an IBFD FSO transceiver for communication among drones. However, these prior studies used LEDs for transmission. In this work, we consider lasers with much narrower divergence angles and beam widths offering high bandwidth but requiring more careful handling of the LOS link perturbations due to mobility.

To improve link quality and provide higher throughput, a multi-transmitter design with directional propagation characteristics over same link can be deployed for FSOC, especially to achieve higher aggregated bandwidth and link robustness due to spatial diversity [15]. Bilgi *et al.* reported that FSO mobile ad-hoc networks (FSO-MANETs) can be designed using optical antennas in spherical shapes, which can achieve angular diversity, spatial reuse, and multi-element incorporation [16]. Alignment and mobility issues of multi-element FSO transceivers were analyzed and modeled by Kaadan *et al.* [17].

B. Laser-based FSOC System Applications

FSOC systems can be categorized based on optical link range and location of deployment. Short-range systems can be very useful for indoor applications and utilize the wider divergence angle of LEDs to establish optical links. However, outdoor settings require narrower beam transmitters and susceptibility to atmospheric turbulence and instability of the mobile platform. Desai *et al.* demonstrated a medium range FSOC system between stationary devices located 500 m to 5 km apart [18]. Furthermore, 72 Mbps to 2.88 Gbps data rate has been demonstrated for near-Earth communications using FSOC systems in the NASA project Laser Communications Relay Demonstration [19]. Before shutting down the campaign in March 2021, the Google Project Loon provided Internet access to remote areas as part of hurricane disaster relief by using a network of balloons at 20 km above sea level through long-range FSOC [2]. Recently, laser inter-satellite links between two LEO Starlink satellite has been reported and deployed which can be a crucial component in achieving low-latency communication paths for next generation satellite networks [3]. However, in this work we focus on short to medium range FSO links with limitations on size, weight, and power (SWaP) to achieve low-altitude laser links for massive network deployment.

III. Multi-Element Full-Duplex FSO Transceiver: Theoretical Background

We demonstrated an IBFD-FSO system prototype implementated by method of isolation in our previous work [5]. In this section, we will present the design methodology and tiling of the elements on the transceiver plane to optimize performance, such as IBFD communication throughput. We used traditional optimization techniques to find the optimum number of transmitters and utilized a genetic algorithm to tile those in a fashion that gives uninterrupted performance even in the presence of vibration.

A. Layout Optimization by Tiling

To determine the optimum transceiver layout, we developed a MATLAB simulation tool to characterize the optical link by incorporating beam characteristics and propagation losses, such as atmospheric turbulence and self-interference. For this simulation, we used 50 m long FSO channel between two UAVs communicating in IBFD mode using wavelength λ = 900 nm. The transceiver size is set to 10 cm $\times$ 10 cm.

Signal-to-Interference-plus-Noise Ratio (SINR) characterizes the quality of a communication system as well as it is the performance parameter for a transceiver. Considering an FSO link established using transceivers A and B, each with a single transmitter having a divergence angle of θ and a single receiver having a detection area of A_{det}, SINR can be written for node A as [20]

$$SINR_A = \left[\frac{P_B L_z(d,\lambda) A_{det} \cos(\phi \pm \delta)}{(\tan\theta)^2 4d^2 (N_T + \Gamma_{SA})}\right]^2, \qquad (1)$$

where P_B is the transmit power at node B, d is the link distance, and $L_z(d,\lambda)$ is the free-space loss parameter for a link distance of d. ϕ is the pointing error angle when the transceivers are perfectly aligned, and δ is the 'vibration angle' which is the additional pointing error due to vibration on the mobile transceivers.

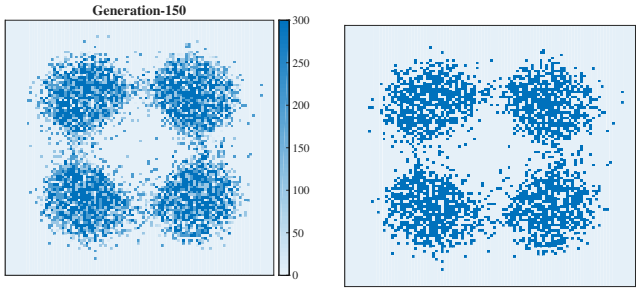

Fig. 1. (a) Heatmap of transmitter locations, and (b) optimized transmitter locations on a 100 × 100 transceiver grid using genetic evolution after generation 150 with 20% fit population with vibrational effect.

For a multi-element FSO transceiver with N transmitters having θ divergence angle each and m receivers with detection area of A_{det}, SINR for node A can be expressed as

$$SINR_A = \sum_{i=1}^{N} \sum_{j:j\in\mathcal{F}_i} \left[\frac{P_{B,i} L_z(d,\lambda) A_{det} \cos(\phi_j \pm \delta_j)}{(\tan\theta)^2 4d^2 (N_T + \Gamma_{SA})} \right]^2, \quad (2)$$

where i and j denote the index of transmitter and receiver, respectively. $P_{B,i}$ denotes the transmit power at transmitter i at node B. Each transmit beam projects a beam footprint on the transceiver plane and only covers a subset of the available receivers in a transceiver. $\mathcal{F}_i$ represents the set of receivers that falls within the beam footprint of transmitter i. ϕ_j and δ_j are the pointing error and the vibration angles on the beam arriving at receiver $j \in \mathcal{F}_i$. N_T is the noise equivalent power and Γ_{SA} is the residual SI power.

To determine the number of the transmitters required to optimize the layout design, we simulated the FSO link by varying the transmitter count. As the position and count of the transmitters are varied, a pointing loss adds to the overall loss parameters. This additional loss degrades the performance of the optical link. We further investigated the link performance based on transmit power and divergence angle of the transmitter to observe the variation on SINR. Based on the simulation, we observe that the SINR of the optical link is highest when 22% of the transceiver area is used as transmitter and 78% area is dedicated for receivers [10].

To determine the optimum position of the transmitters, we devised a genetic algorithm approach with smaller segment area. We divided the transceiver plane into 100×100 smaller segments and assigned 22% of the segments as transmitter. In our developed algorithm, we have randomly generated $5,000$ different sets by placing the transmitters in different segments to start the process. After calculating the SINR for each set, we selected best 10% of the sets, which we named 'fit population'. We used these fit population sets to generate the population of $5,000$ sets for the next generation by crossover technique. This process of generating population set and calculating SINR to determine fit population for the next generation is iterated until we achieve the best optical link performance. SINR is calculated for each set in the generation and average SINR is compared with the previous generations. If the average

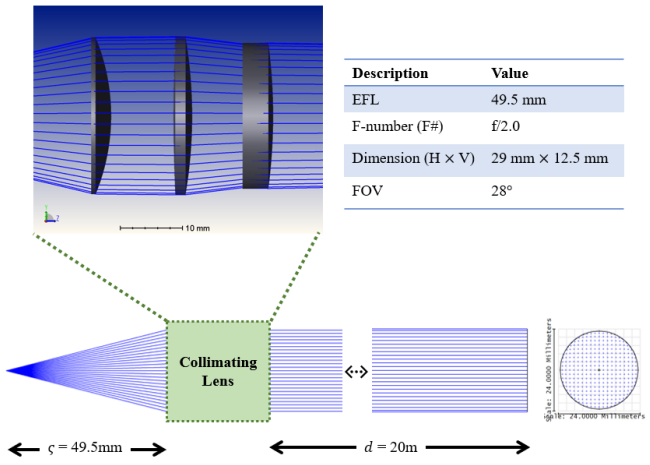

Description	Value
EFL	49.5 mm
F-number (F#)	f/2.0
Dimension (H × V)	29 mm × 12.5 mm
FOV	28°

Fig. 2. Fixed effective focal length lens for FSO system.

SINR of the generations does not improve at least 0.001% for three (3) consecutive generations, we assume the solution converges. Once we converge to a solution, we can generate a heatmap of the optimized 'fit population' to determine the locations where we place the transmitters, as shown in Fig. 1. The converged heatmap shows that the transmitter locations are more clustered in four lobes located midway towards the corners of the transceiver plane from the center.

B. Circuit Design for Transmitter and Receiver Threads

We discuss about the circuit design considerations for the 10×10 transceiver prototype for multi-element FSO link by incorporating SWaP constraints [10]. The electrical circuit associated with the transmitter and receiver thread are designed separately. However, both of the circuits interact with the controller and laid out on the same printed circuit board (PCB) in accordance to the layout simulated in the previous section.

As shown in previous section, the optical simulation provides best link performance if there are 22 transmitters in the 10×10 transceiver array. However, to distribute the transmitter along multiple routes and balance the current supplied to each transmitter, we choose to use 24 transmitters. The transmitters are clustered in 4 areas as shown in Fig. 1, having 6 transmitters in each cluster. In our circuit, we distributed 3 transmitters per path and defined 8 paths for transmit thread. The combination of all the transmitting elements' aggregate power will give a better SNR for the receiving end. The second reason why the 8×3 layout was chosen due to voltage and current driving requirements of the transmitter circuit elements (narrow band LEDs).

For the receiver circuit design, the baseline layout was chosen roughly 10×10. This routing path is chosen for three reasons: First, it is easier for routing to one path per column, with more or less elements per path as needed to match the array. Second, the RC delay may deteriorate the received signal. However, allowing multiple path to dissipate the accumulated charges for the receiver elements ensures each bit is received

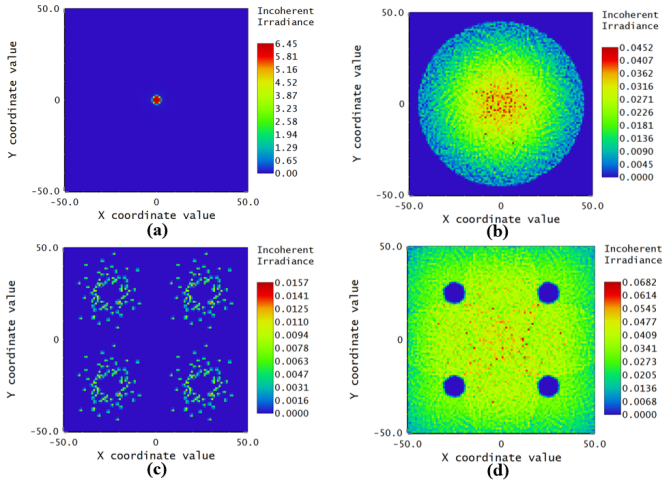

Fig. 3. Optical beam footprint for (a) single transmitter collimated beam ($\Delta\zeta = 0$), (b) single transmitter defocused beam ($\Delta\zeta = 0.8$ mm), (c) four transmitters collimated beam ($\Delta\zeta = 0$), and (d) four transmitters defocused beam ($\Delta\zeta = 0.8$ mm).

without any residual charges in the circuit. Third, the overall capacitance of the circuit remains relatively low if we combine the components in series and parallel combination and we can control the effective capacitance of the receiver circuit. The detail design, circuit diagram, and performance analysis by considering SWaP constraints are presented in our previous work [10].

IV. Defocal Lens Assembly for Transmitters

When parallel (or collimated) light rays from an infinitely distant source falls on a lens system, there are three possible outcomes: First, the parallel rays converge to a real-point outside the lens system; second, the light rays appear to diverge from a point within the lens system; and third, they emerge as parallel (or collimated) rays after the lens system with a little different characteristics compared to the incident rays. In the first two cases, the lens system has a finite focal length and field-of-view (FOV). These systems are called focal systems. On the other hand, the system in the third case does not have finite focal length, or one can say the light rays converge or diverge at a infinite length. This system is called afocal lens system. The direction of the ray path is reversible. Hence, for the first case scenario, if a diverging point source is placed at a focal length of a lens system, the output light rays appears to be parallel (or collimated), as shown in Fig. 2. We utilize these characteristics to design a lens assembly for the transmitters for medium range FSOC.

To improve the performance of the overall optical system, one of the major parameters that requires improvement is optical coupling efficiency (η_{OC}) [21]. Generally, coupling efficiency indicates how much transmitted power can be coupled into the receiver. The expression for η_{OC} can be given as follows

$$\eta_{OC} = \eta_T \eta_{ch} \eta_R, \tag{3}$$

where η_R is the transmitter outcoupling efficiency, η_{ch} is the channel coupling efficiency that includes atmospheric attenuation losses and perturbations, and η_R is the receiver efficiency that includes power collected by the receiver area and coupling optical power into electrical circuits. Losses incurred during the beam propagation through free-space are accounted for in the coupling term η_{ch}. Atmospheric absorption, scattering, and turbulence are the major factors to deteriorate beam quality and directionality. However, these effects are minimum when we consider clear weather, higher visibility, and temperature gradient is small. These effects may become prominent for long-range FSOC [22].

In paraxial analysis, the transmitter is placed at the focal point of the lens system on the optical axis. If the emission distribution is described by $J_T(\beta)$, where J_T is normalized to emission into 2π steradians of a hemisphere and β is the angle from zenith, the transmitter then can be approximated by [21]

$$\eta_T = \int_0^{\beta_{max}} \int_0^{2\pi} J_T(\beta) d\beta d\phi, \tag{4}$$

where $\beta_{max} = \tan^{-1}(1/2F_T)$ is the angle of the marginal rays to the edge of the lens and F_T is the F-number of the lens. The coupling efficiency of the receiver (η_R) can be described as the ratio of the power collected by the receiver to the power that arrives at the receiver plane. If the intensity distribution of the beam at the receiver plane is defined as $J_R(d)$, η_R can be given by

$$\eta_R = \frac{\int\int \Big(J_R(d) \circledast A_R \Big)}{\int\int \Big(J_R(d) \circledast A_{BF} \Big)}, \tag{5}$$

where d is the optical link distance, A_R is the effective receiver area, and A_{BF} is the beam footprint at the transceiver plane. This coupling efficiency cannot be represented by the ratio of the receiver area and beam footprint, as the intensity of a Gaussian beam varies within the beam cross section.

To observe the relation between the optical link distance, coupling efficiency, defocused beam footprint, and vibration tolerance, we developed a lens assembly in Zemax OpticStudio with paraxial approximation. The lens assembly was designed in a fashion so that the light rays coming out of the lens are collimated and hence can be useful for longer optical range. The lens prescription was optimized using sequential mode in Zemax. The spot size of the beam on the receiver plane is 11 mm and most of the power is contained within the beam width, as shown in Fig. 3(a). But if we consider transceiver design, this beam will fall only on the transmitter on the other side and none of the power arriving at the receiver plane will be converted into signal. Hence, we deliberately defocus the beam by changing the distance (ζ) between transmitter and lens assembly. A very small offset of $\Delta\zeta = 0.8$ mm can lead to a much bigger beam footprint at the receiver plane, as shown in 3(b). Now, as outlined in the previous section, we have four cluster of transmitters on the transceiver plane. We simulated the transceiver plane power coupling by using non-sequential

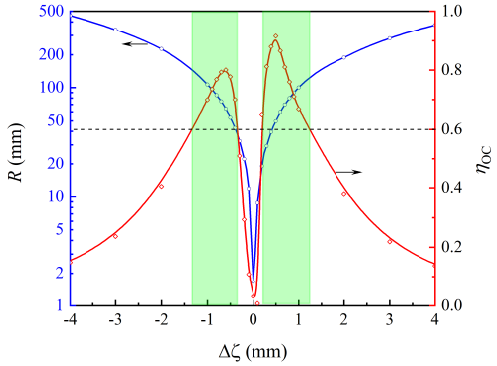

Fig. 4. Beam width radius, R, (blue line) and optical coupling efficiency, η_{OC}, (red line) for optical link range, $d = 20$ m.

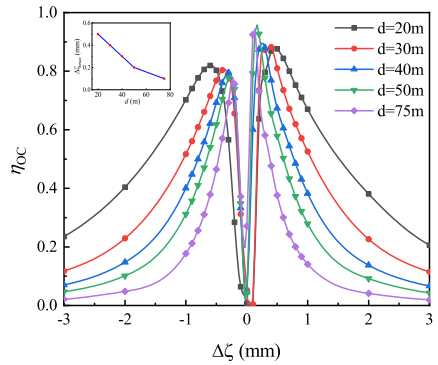

Fig. 6. Optical coupling efficiency, η_{OC}, for different link range, d. Inset: Defocused length ($\Delta\zeta_{max}$) corresponding to the maximum coupling effieicny for different link range, d.

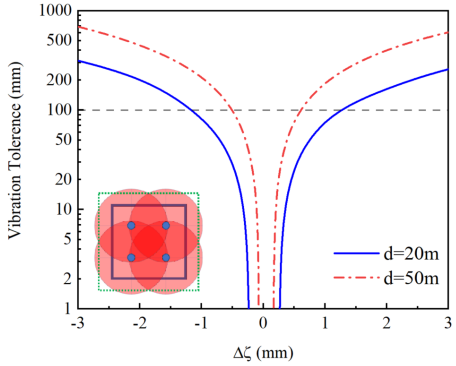

Fig. 5. Vibration tolerance for defocused lens system for $d = 20$ m and $d = 50$ m.

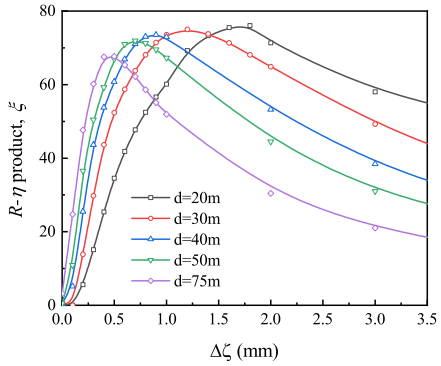

Fig. 7. Variation of trade-off parameter, ξ, corresponding to defocused length, $\Delta\zeta$ for different optical link range, d.

environment in Zemax. For both collimated (Fig. 3(c)) and defocused (Fig. 3(d)) cases, beam footprint shows how much power would be coupled into the receiver.

V. Results and Discussion

We present a defocused lens system for the transmitter of the laser-based IBFD FSOC link. We designed a fixed focal length lens system with adjustable distance between transmitter and lens assembly (ζ). The adjustable ζ can be effective and advantageous for three reasons: First, the controller can optimize the beam footprint radius by implementing feedback algorithm so that it can cover maximum receiving area and couple maximum power to the receiving end. Second, with the variation of optical link range, defocusing distance ($\Delta\zeta$) is different. The adjustability of the $\Delta\zeta$ gives an optimum operating condition over a wide window of optical range. Third, mobile platforms tend to experience loss of communication due to vibration, sway, and tilt. Use of lasers as transmitters makes it even harder to maintain the optical link. By using adjustable $\Delta\zeta$, we can provide robustness and tolerance to vibration and sway. However, this robustness to vibrations comes with a trade-off. We can increase tolerance by increased defocus and larger beam footprint, which leads to distributed intensity and lower coupling efficiency. We define a term (ξ) to measure the trade-off between beam footprint radius (R) and coupling efficiency (η_{OC}), where $\xi = R \times \eta_{OC}$. Larger beam footprint radius gives much better vibration tolerance of the system, but at the same time received power is compromised. The intensity of light has Gaussian distribution across the beam footprint. As the receiver area is constant, by increasing R effectively reduces η_{OC}. By maximizing ξ values, we can ensure optimum operating condition of FSOC.

We start our design by optimizing the lens assembly, defined in Fig. 2, in the sequential environment in Zemax. We determine the beam footprint radius (R) of the beam spot on the receiver plane. As we can see from Fig. 4, the radius increases with the defocusing distance ($\Delta\zeta$) for a link distance of $d = 20$ m and corresponding ray trace diagram is also shown in Fig. 2. The corresponding vibration tolerance margin is also calculated and shown in Fig. 5. The tolerance of the system in terms of the defocusing distance corresponds to the beam footprint diagram. In the beam footprint (area of the dotted green box in Fig. 5 inset), the additional length in either horizontal or vertical direction represents the tolerance length.

After we finalize the lens system design based on the collimation of light rays, we convert our lens design into non-sequential environment. Based on the simulation results presented in previous section, we position four (4) transmitters

on the transceiver plane and rest of the area is defined as receiver. The distance between two transceiver planes is varied from 20 m to 75 m. The coupling efficiency is calculated based on the received power by the receiver. Figure 4(red line) shows the coupling efficiency with respect to defocusing distance ($\Delta\zeta$). When $\Delta\zeta = 0$ or the incoming beam to the receiver plane is collimated, least amount of power is coupled into receiver, as most the power is perfectly aligned with the transmitter on the transceiver plane. But as the defocusing starts to kick in, coupled received power also increases as long as the beam radius falls within the transceiver plane. When the beam radius at the receiver plane becomes significantly larger than transceiver area, coupling efficiency goes down again. Even though Gaussian beam concentrates more power at the center of the beam cross-section, as the beam radius increases, power starts to distribute over larger area and effective coupling goes down. We further investigate the effect of optical link range (d) on the coupling efficiency. The maximum coupling efficiency (η_{max}) remains relatively constant over wide window of optical range (from 20 m to 75 m). However, η_{max} occurs at different defocusing distance ($\Delta\zeta_{max}$) for different d values. Figure 6 shows the coupling efficiency for different d values at different $\Delta\zeta$ positions. We have also shown how the position of $\Delta\zeta_{max}$ varies over a window of optical link range.

Finally we calculate the value of ξ to determine the optimum operating defocusing distance, $\Delta\zeta$. Figure 7 shows the trade-off parameter, ξ, with respect to $\Delta\zeta$ for different optical link range, d. We can determine the optimum value of $\Delta\zeta_{opt}$ from these plots. We can observe that $\Delta\zeta_{opt}$ is smaller for higher d values, as non-collimated beam has larger beam footprint for longer link range. As a result, coupling efficiency drops much faster compared to smaller link range, as can be observed from Fig. 6 as well. These simulation results provide a guideline for designing fixed effective focal length lens system and how defocusing can be utilized to optimize coupling efficiency and vibration tolerance for a mobile FSOC link.

VI. Conclusion

In conclusion, we presented a complete design guideline for in-band full-duplex FSO transceiver for short to medium range mobile FSOC links. We incorporated atmospheric attenuation and turbulence effect in designing a multi-element FSO transceiver, which shows maximum SINR performance when 22% of the transceiver area is used for transmitter and generates a layout for optimum performance by using genetic algorithm. We outlined how these multiple optical elements, namely transmitters and receivers, are connected in the electrical circuit by considering SWaP constraints. And finally, we developed a transmitter lens assembly with fixed effective focal length to maximize the optical coupling efficiency and vibration tolerance for a mobile FSOC link by adjusting defocusing length. We propose a lens system with 49.5 mm EFL, F/2, and FOV of 28° for each transmitter cluster which gives a coupling efficiency of up to 57% and vibration tolerance of 11.5 cm when the link range is $d = 50$ m.

References

[1] M. Khan, M. Yuksel, and G. Winkelmaier, "GPS-free maintenance of a free-space-optical link between two autonomous mobiles," *IEEE Transactions on Mobile Computing*, vol. 16, no. 6, pp. 1644–1657, 2017.

[2] B. Moision, B. Erkmen, E. Keyes, T. Belt, O. Bowen, D. Brinkley, Csonka *et al.*, "Demonstration of free-space optical communication for long-range data links between balloons on project loon," in *Free-Space Laser Communication and Atmospheric Propagation XXIX*, vol. 10096. SPIE, 2017, p. 100960Z.

[3] A. U. Chaudhry and H. Yanikomeroglu, "Laser intersatellite links in a starlink constellation: A classification and analysis," *IEEE Vehicular Technology Magazine*, vol. 16, no. 2, pp. 48–56, 2021.

[4] M. A. Khalighi and M. Uysal, "Survey on free space optical communication: A communication theory perspective," *IEEE communications surveys & tutorials*, vol. 16, no. 4, pp. 2231–2258, 2014.

[5] A. F. M. S. Haq, M. R. Khan, and M. Yuksel, "A prototype of in-band full-duplex free-space optical transceiver," in *2018 IEEE International Symposium on Local and Metropolitan Area Networks (LANMAN)*. IEEE, 2018, pp. 112–113.

[6] P. Deng, T. Kane, and O. Alharbi, "Reconfigurable free space optical data center network using gimbal-less mems retroreflective acquisition and tracking," in *Free-Space Laser Communication and Atmospheric Propagation XXX*, vol. 10524. SPIE, 2018, p. 1052403.

[7] B. Winker, M. Mahajan, and M. Hunwardsen, "Liquid crystal beam directors for airborne free-space optical communications," in *2004 IEEE Aerospace Conference Proceedings (IEEE Cat. No. 04TH8720)*, vol. 3. IEEE, 2004.

[8] R. Fatemi, A. Khachaturian, and A. Hajimiri, "A low power pwm optical phased array transmitter with 16° field-of-view and 0.8° beamwidth," in *2018 IEEE Radio Frequency Integrated Circuits Symposium (RFIC)*. IEEE, 2018, pp. 28–31.

[9] T. Koonen, F. Gomez-Agis, F. Huijskens, K. A. Mekonnen, Z. Cao, and E. Tangdiongga, "High-capacity optical wireless communication using two-dimensional ir beam steering," *Journal of Lightwave Technology*, vol. 36, no. 19, pp. 4486–4493, 2018.

[10] P. De La Llana, A. S. Haq, and M. Yuksel, "Design of a multi-element fso transceiver array for mobile communication links," in *Free-Space Laser Communications XXXIII*, vol. 11678. SPIE, 2021, p. 1167805.

[11] K. Wang, A. Nirmalathas, C. Lim, K. Alameh, and E. Skafidas, "Full-duplex Gigabit indoor optical wireless communication system with CAP modulation," *Photonics Tech. Lett.*, vol. 28, no. 7, pp. 790–793, 2016.

[12] C. W. J. Oh, Z. Cao, E. Tangdiongga, and T. Koonen, "10 Gbps all-optical full-duplex indoor optical wireless communication with wavelength reuse," in *OFC*. Optical Society of America, 2016, pp. Th4A–6.

[13] B. E. Johnson, T. A. Lindsay, D. L. Brodeur, R. E. Morton, and M. A. Regnier, "Wide-angle, high-speed, free-space optical communications system," Oct. 25 1994, uS Patent 5,359,446.

[14] A. F. M. S. Haq, M. Khan, and M. Yuksel, "Asynchronous LOS discovery algorithm for aerial nodes using in-band full-duplex transceivers," in *Proceedings of the 15th International CoNEXT*. ACM, 2019.

[15] J. Akella, M. Yuksel, and S. Kalyanaraman, "Multi-element array antennas for free-space optical communication," in *2nd IFIP International Conference on Wireless and Optical Communications Networks*. IEEE, 2005, pp. 159–163.

[16] M. Bilgi and M. Yuksel, "Multi-element free-space-optical spherical structures with intermittent connectivity patterns," in *IEEE INFOCOM Workshops 2008*. IEEE, 2008, pp. 1–4.

[17] A. Kaadan, H. H. Refai, and P. G. LoPresti, "Multielement FSO transceivers alignment for inter-UAV communications," *Journal of Lightwave Technology*, vol. 32, no. 24, pp. 4785–4795, 2014.

[18] A. Desai and S. Milner, "Autonomous reconfiguration in free-space optical sensor networks," *IEEE Journal on Selected Areas in Communications*, vol. 23, no. 8, pp. 1556–1563, 2005.

[19] B. Edwards, "Overview of the laser communications relay demonstration project," in *SpaceOps 2012*, 2012, p. 1261897.

[20] J. W. Giles and I. N. Bankman, "Underwater optical communications systems. part 2: Basic design considerations," in *MILCOM 2005-2005 IEEE Military Comm. Conf.* IEEE, 2005, pp. 1700–1705.

[21] S. S. Polkoo and C. K. Renshaw, "Imaging-based beam steering for free-space optical communication," *Applied optics*, vol. 58, no. 13, pp. D12–D21, 2019.

[22] L. C. Andrews and R. L. Phillips, "Laser beam propagation through random media." SPIE, 2005.